

## Structure in the Pion-Proton Total Cross Section between 2 and 7 GeV/c\*

A. CITRON,<sup>†</sup> W. GALBRAITH,<sup>‡</sup> T. F. KYCIA, B. A. LEONTIC, R. H. PHILLIPS,  
A. ROUSSET,<sup>§</sup> AND P. H. SHARP<sup>||</sup>

Brookhaven National Laboratory, Upton, New York

(Received 29 September 1965; revised manuscript received 13 January 1966)

The total cross sections of  $\pi^\pm$  on protons in the momentum interval 2 to 7 GeV/c have been measured with high precision. The error fluctuations from point to point vary between 10 and 25  $\mu$ b. Two new pion-nucleon resonances, one in each of the two isotopic states, have been found at the following mass values:  $M_{1/2}=2.65\pm 0.01$  GeV and  $M_{3/2}=2.85\pm 0.01$  GeV. A search for other resonances at higher momenta is discussed.

### I. INTRODUCTION

A MEASUREMENT of the total cross section of  $\pi^\pm$  mesons on protons has in the past afforded a good method for detecting the presence of the  $\pi$ -nucleon resonances. The two most important advantages of this method lie in the possibility of obtaining data with small statistical errors (i.e., large numbers of events) and in the ease with which effects due to the two isotopic spin states  $T_{1/2}$  and  $T_{3/2}$  can be separated. Resonances with masses around 1.5 GeV were comparatively easy to observe because their heights, relative to the background, were large, typically greater than 10 mb. The highest mass  $\pi$ -nucleon resonances published hitherto<sup>1</sup> were more difficult to detect because their heights were only some few millibarns, and it was clear from other work<sup>2</sup> at higher momenta that any structure which might exist in the total cross section above the 2.6-GeV/c  $\pi^+p$  resonance was likely to be less than 1 mb in height.

For this reason, a new experimental search for resonances in the 2.5–7.0 GeV/c range had to be very precise. Improved statistics result in higher accuracy, and errors in the absolute value can be tolerated if these are not energy-dependent, but any drift which may produce a structure in total cross section has to be carefully avoided.

In the present experiment the fluctuations from point to point varied between 10 and 25  $\mu$ b in the momentum range 2.5 to 7.0 GeV/c. Two new pion-nucleon resonances, one in each of the two isotopic states, were found at the following mass values:  $M_{1/2}=2.65\pm 0.010$  GeV and  $M_{3/2}=2.85\pm 0.012$  GeV. A search for further resonances at higher momenta is described and some

indication of the existence of two such resonances is discussed.

### II. PRINCIPLE OF A TRANSMISSION EXPERIMENT

The method used for measuring total cross sections was that of a standard good-geometry transmission experiment. A beam of particles is obtained from an accelerator and the  $\pi$  mesons are identified by means of a differential Čerenkov counter. The beam, defined by an input telescope, passes through either a hydrogen or dummy target and converges to a focus at which point a number of transmission counters (detectors), subtending a range of solid angles at the target, are situated. The detectors are followed by an iron absorber for  $\pi$  mesons followed by a scintillation counter which is in anticoincidence with the detectors. The effect of this counter is to veto, in principle, all muons passing through the iron. For a full discussion of this point, see Sec. III D.

Define the transmission rate  $R_i$  as

$$R_i = T_i A / S, \quad (1)$$

where  $S$  is the number of particles incident on the target and detected by the input telescope,  $T_i$  is the number of such particles transmitted by the target striking the detector  $i$ , and  $A$  is the fraction of transmitted particles not vetoed by the muon anticoincidence counter. This rate is measured for a full and for an empty hydrogen target of identical geometry and composition. The transmission rates  $R_{if}$  and  $R_{ie}$  for full and empty targets, respectively, can also be written in the form

$$R_{if} = B_{if} \exp(-\sigma_i \rho L N / M), \quad (2)$$

$$R_{ie} = B_{ie}, \quad (3)$$

where  $\sigma_i$  is the "total cross section" as observed with detector  $i$ ,  $\rho$  is the density of the hydrogen,  $L$  is the length of the hydrogen column,  $N$  is Avogadro's number, and  $M$  is the atomic weight of hydrogen;  $B_{if}$  and  $B_{ie}$  measure the attenuation in the target envelope, in the last counter of the input telescope and in all counters between the target and detector  $i$ . They also include any counting inefficiency.

We now make the assumption that

$$B_{if} = B_{ie} = B_i, \quad (4)$$

\* Work done under the auspices of the U. S. Atomic Energy Commission.

<sup>†</sup> Permanent address: CERN, Geneva, Switzerland.

<sup>‡</sup> Permanent address: Atomic Energy Research Establishment, Harwell, England.

<sup>§</sup> Permanent address: Ecole Polytechnique, Paris, France.

<sup>||</sup> Permanent address: Atomic Energy Research Establishment, Harwell, England.

<sup>1</sup> A. N. Diddens, E. W. Jenkins, T. F. Kycia, and K. F. Riley, Phys. Rev. Letters **10**, 262 (1963).

<sup>2</sup> W. F. Baker, E. W. Jenkins, T. F. Kycia, R. H. Phillips, A. L. Read, K. F. Riley, and H. Ruderman, in *Proceedings of the Sienna International Conference on Elementary Particles, 1963*, edited by G. Bernadini and G. P. Puppi (Societá Italiana di Fisica, Bologna, 1963).

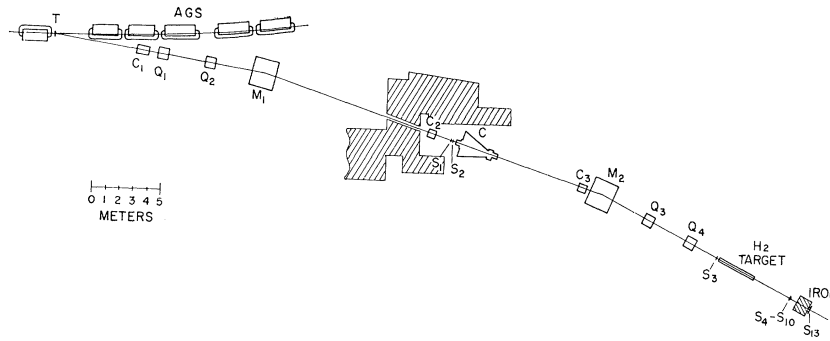


FIG. 1. Experimental arrangement at Brookhaven Alternating Gradient Synchrotron (AGS). T, beryllium target; C<sub>1</sub>-C<sub>3</sub>, collimators; Q<sub>1</sub>-Q<sub>4</sub>, quadrupoles 20.3-cm diam aperture, 122 cm long; M<sub>1</sub>, M<sub>2</sub>, bending magnets 15.2-cm gap, 183 cm long; S<sub>1</sub>-S<sub>8</sub>, scintillation counter telescope; C, Čerenkov counter; S<sub>4</sub>-S<sub>10</sub>, transmission counters; S<sub>13</sub>, anticounter.

i.e., that all losses are the same for full and empty targets. As far as electronic circuit losses are concerned, this means that they should not vary with time. It also means that losses should not be dependent on the difference observed in counting rates for full and empty targets due to the absorption of pions in the hydrogen and that the energy loss suffered by the pions in the hydrogen (about 90 MeV) does not change the absorption probability in parts of the apparatus between the hydrogen and detector *i* appreciably.

The cross section  $\sigma_i$  is then found from

$$\sigma_i = (M/\rho LN) \ln(R_{ie}/R_{if}) \quad (5)$$

so the quantity  $B_i$  disappears.

This cross section gives the probability for a pion not to be transmitted to detector *i*. Particles suffering a scattering through a sufficiently small angle to be intercepted by detector *i* are counted as transmitted. So we have

$$\sigma_i = \sigma - \int_0^{\Omega_i} \frac{d\sigma(\theta)}{d\Omega} d\Omega, \quad (6)$$

where  $\sigma$  is the total cross section we wish to measure, and  $\Omega_i$  is the mean solid angle subtended by the detector *i*.  $d\sigma(\theta)/d\Omega$  is the differential cross section for the emission of at least one charged particle by an elastic or inelastic process into the direction defined by the (small) polar angle  $\theta$ .

Let the dimensions of all detectors be small enough that the diffraction peak can be regarded as flat over the angular region subtended. With the further assumption that the angular distribution for all other nuclear phenomena is also flat within this same region and disregarding, for the moment, multiple Coulomb scattering, we can write Eq. (6) as follows:

$$\sigma_i = \sigma - (d\sigma/d\Omega)\Omega_i. \quad (7)$$

Thus, plotting  $\sigma_i$  against  $\Omega_i$  we obtain a straight line, as long as our assumptions are correct. The intercept with the ordinate gives the desired total cross section; the slope gives the forward differential cross section as defined above. For the largest detectors and for high momenta we expect a deviation from a straight line because the differential cross section starts falling off.

For the smallest detectors and for lower momenta the multiple Coulomb scattering gives a deviation from a straight line. These two phenomena were indeed observed, but for hydrogen there always remained a range of solid angles, comprising at least three transmission counters, for which the plot is a straight line within the statistical errors of the individual points. This is to be expected on the basis of the published behavior of the differential elastic cross section.<sup>3</sup> It was also verified that, at least in the case of scattering of 8-GeV/*c*  $\pi^+$  in hydrogen, the forward differential cross section as we observed it (counting all charged particles emitted into the solid angle under consideration) falls off with an exponent having half the value of that for the elastic case.<sup>4</sup>

A discussion of the effect of the Coulomb interference on the determination of the total cross section is given in the Appendix.

### III. APPARATUS AND PERFORMANCE

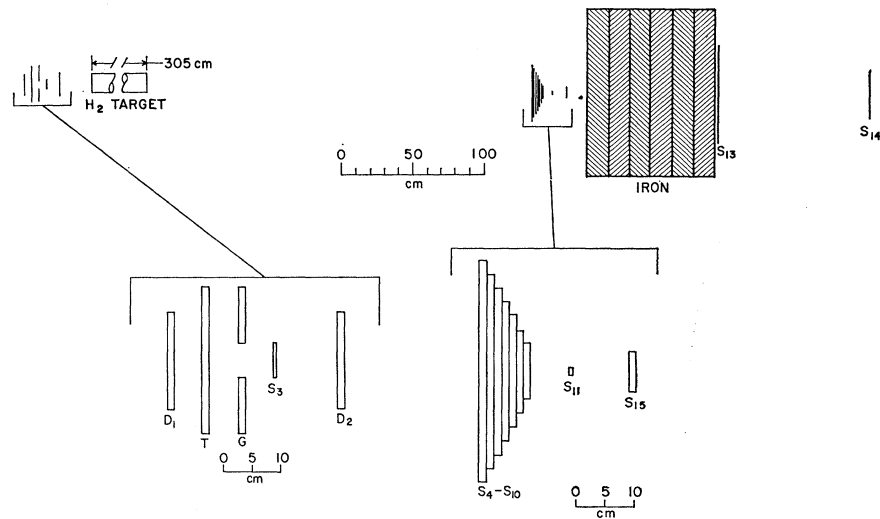
#### A. The Beam

The beam (Figs. 1 and 2) is of the conventional symmetric design. It originates from a beryllium target 0.8 mm thick and 12.5 mm long, located in a straight section of the AGS and oriented at 4.5° to the circulating proton beam (along the axis of a beam for another experiment). This target is viewed at 9° to the proton beam, that is at 4.5° with respect to the target axis. Collimator 1 limits the beam in both planes and acts as an aperture stop for the first half-section of the beam. The pair of quadrupole lenses Q<sub>1</sub> and Q<sub>2</sub> form at collimator 2 in both the horizontal and vertical planes an image of the production target after a 9° deflection in the bending magnet M<sub>1</sub>. Collimator 2 and M<sub>2</sub> define the momentum; the horizontal width of C<sub>2</sub> is 2.2 cm giving a calculated momentum spread of  $\pm 0.5\%$ . Collimator 3 is designed to prevent particles which suffered large multiple scattering in the Čerenkov counter from re-scattering off magnet-pole faces and vacuum pipes. All secondaries created in collimators 2 and 3 and in the

<sup>3</sup> K. J. Foley, S. J. Lindenbaum, W. A. Love, S. Ozaki, J. J. Russell, and L. C. L. Yuan, *Phys. Rev. Letters* **11**, 425 (1963).

<sup>4</sup> Aachen, Berlin, CERN Collaboration (private communication from D. R. O. Morrison).

FIG. 2. Detailed layout of apparatus, plan view. D<sub>1</sub>, D<sub>2</sub>, scintillation counters to reduce accidental coincidences; T, scintillation counter to control dead-time effects; G, scintillation counter to eliminate particles outside the defined beam; S<sub>3</sub>, final scintillation counter in beam telescope; S<sub>4</sub>-S<sub>10</sub>, scintillation counter for beam alignment; S<sub>11</sub>, scintillation counter in anticoincidence to eliminate muons; S<sub>14</sub>, S<sub>15</sub>, scintillation counters for counter-efficiency checks.



Čerenkov counter are swept away by magnet  $M_2$  which is also used to recombine momenta at the final image. This second bending magnet and the pair of quadrupole lenses,  $Q_3$  and  $Q_4$ , form a final image at the transmission counters,  $S_4$ - $S_{10}$ .

Whenever the momentum was changed,  $M_2$  and the quadrupoles were set at the calculated field values. Then the small counter  $S_{11}$  was switched into coincidence with the input telescope and the current in  $M_1$  was adjusted to give maximum counting rate. The magnetic field in the bending magnet  $M_2$  was monitored continuously to  $\pm 0.05\%$  by means of a nuclear-resonance flux meter. The absolute value of the momentum was verified with the floating-wire method and the result agreed to within 1% with that calculated using measurements by Danby and Jackson.<sup>5</sup> It should be noted that the momentum values quoted in our data are corrected for the energy loss in half the length (1.5 m) of the hydrogen target, i.e., the momentum quoted is the mean value at the midpoint of the hydrogen target. We thus measure cross sections centered at the quoted value, but averaged over a momentum bite of 100 MeV/c at 2.5 GeV/c and 150 MeV/c at 7.0 GeV/c including the momentum spread determined by collimator 2 plus that caused by energy loss in the target.

Multiple scattering in the hydrogen target makes the extrapolation to zero solid angle more difficult. The larger the spot size of the beam striking the detector in the absence of the hydrogen target the greater is the number of detectors affected by multiple scattering. For this reason it is important to keep the spot size as small as possible. Multiple scattering in air was reduced by vacuum pipes and helium bags.

The main source of widening of the beam is the multiple scattering in the Čerenkov counter. The gas length is 310 cm and the matter it introduces into the

beam is  $0.4 \text{ g cm}^{-2}$  of Al for each window,  $0.7 \text{ g cm}^{-2}$  of glass for the mirror, and  $6 \text{ g cm}^{-2}$  of  $\text{CO}_2$  (at  $10.5 \text{ kg cm}^{-2}$  pressure for 2.5 GeV/c). The corresponding rms scattering angle at 2.5 GeV/c is  $\theta_{\text{rms}} = 4 \text{ mrad}$ . For this reason, this counter and the preceding scintillation counters  $S_1$  and  $S_2$  were placed as near to the momentum collimator as possible where the beam has its maximum divergence ( $\alpha_H = \pm 5 \text{ mrad}$ ,  $\alpha_V = \pm 3 \text{ mrad}$ ). This is not the ideal position for the Čerenkov counter but it gives minimum increase in spot size. The spot size with the hydrogen target removed was measured to be  $1.8 \times 2.5 \text{ cm}$  (full-width at half-height). This is comparable with the spot size due to multiple scattering in the hydrogen target alone, which is calculated to be  $2.25 \times 2.25 \text{ cm}$  for  $\theta_{\text{rms}}$  at a momentum of 3 GeV/c. The presence of the Čerenkov counter does not seriously enlarge the final beam spot.

## B. Counters and Electronics

1. *The counters.* The block diagram of the experiment is shown in Fig. 3; details of the counters are given in Table I. Pulses from all counters are split and fed into two completely independent sets of circuitry. One comprised units commercially available from Chronetics, Inc.; the other, of units somewhat similar in design, manufactured at Brookhaven National Laboratory (HEEP circuitry).

$S_1$ ,  $S_2$ , and  $S_3$  (Fig. 1) are three scintillation counters that defined incident particles in the beam.  $S_1$  and  $S_2$  were situated near the first focus ahead of the Čerenkov counter C, whereas  $S_3$  defined the beam at the entry of the hydrogen target. The G counter, with a hole in its center, detected particles outside the defined beam and its signal was placed in anticoincidence with the beam telescope.

The  $D_1$ ,  $D_2$ , and T counters, located next to  $S_3$ , were used to eliminate accidental and dead time effects; they will be discussed in more detail later.

<sup>5</sup> G. T. Danby, Brookhaven National Laboratory Internal Report GTD-2, (unpublished) and private communication from J. W. Jackson.

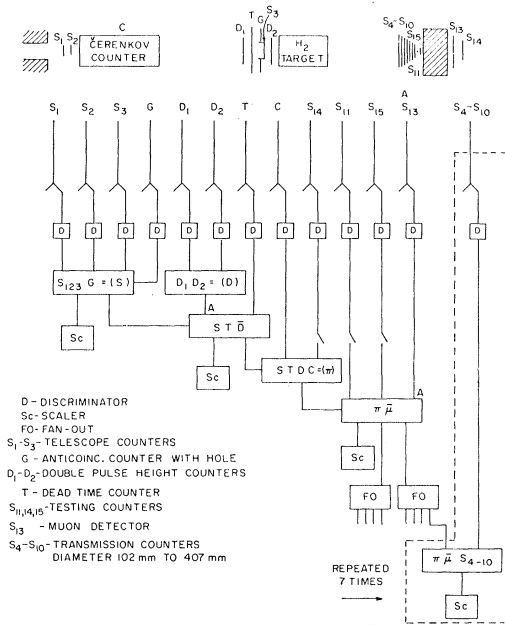


FIG. 3. Block diagram of the counters and electronics circuitry.

The  $\pi$  mesons were selected from the beam by means of a differential gas Čerenkov counter.<sup>6</sup> In setting up the experiment, pressure curves were taken at four momenta 2.5, 3.0, 4.0, and 5.4 GeV/c only. The pressures for other momenta were then set by interpolation and extrapolation.

As a subsidiary test, the pressure of the Čerenkov counter which was optimum at 9.25 kg cm<sup>-2</sup> for 3-GeV/c pions was varied between 8.3 and 10.2 kg cm<sup>-2</sup>. At this momentum, the cross section was measured for each pressure setting over this range to a statistical accuracy of 24  $\mu$ b. No dependence of cross section on the Čerenkov pressure was noticed within this pressure range. Therefore a slight error in the Čerenkov pressure during the data taking is not expected to result in a significant error in the cross section.

The transmission counters S<sub>4</sub>-S<sub>10</sub> were circular and subtended solid angles at the center of the target ranging from 2 to 30 msr. The counters were arranged along the beam direction in order of decreasing radius for two reasons. Firstly, this arrangement allows a determination to be made of the statistical error in the difference between any two partial cross sections. This follows because all the particles counting in the smaller of any pair of transmission counters are common to the larger counter, independent of particle absorption by the transmission counters. The other reason is also due to particle absorption. Since some absorption takes place in each counter, the detection efficiency of the subsequent counters is reduced. In the geometry chosen here, this reduction is independent of whether the beam

is collimated (empty target) or spread out (full target). So this inefficiency does not affect the results. If the counters were assembled in the reverse order, i.e., the smallest counter nearest to the hydrogen target, the second counter would be screened by the first one only in its central part. Therefore, there would be more loss in the empty target case than in the full one. On the other hand, the definition of solid angles is slightly less precise in the arrangement chosen here due to the effect of multiple scattering in the preceding counters. This is, however, a very small effect.

The scintillation counter S<sub>13</sub> situated behind the iron absorber for  $\pi$  mesons detected muons not rejected by the Čerenkov counter C or those due to decay of  $\pi$  mesons after the Čerenkov counter. Its signal was put in anticoincidence with the signal denoting a  $\pi$  meson (Fig. 3). The scintillator had a diameter of 711 mm in order to detect muons that underwent large multiple scattering effects in the iron. The effect of this counter is discussed in more detail in a later section.

Scintillation counters S<sub>11</sub>, S<sub>14</sub>, and S<sub>15</sub> were "test counters." The S<sub>14</sub> counter was used to determine the veto efficiency of the S<sub>13</sub> counter. The S<sub>11</sub> and S<sub>15</sub> counters are discussed elsewhere.

2. *Electronics stability.* The decisive importance of long- and short-term stability of the electronic circuitry is obvious. In order to check this point, the results obtained with the Chronetic circuitry were compared with those obtained with the HEEP circuitry with the two sets being operated under identical conditions. In this way, any fluctuation of the electronics in one set shows up as a deviation from the other. The cross section measured with one set usually differed from the other by a constant amount of less than 125  $\mu$ b and a fluctuation less than  $\pm 15 \mu$ b. In other phases of the experiment, one

TABLE I. The counters.

Counter	Dimensions (mm)		Thickness (mm)	Role
	H	W		
S <sub>1</sub>	35	63	9.5	Beam telescope
S <sub>2</sub>	41	73		
S <sub>3</sub>	135	61		
D <sub>1</sub> , D <sub>2</sub>	178	178	13	Elimination of double particles
T	356	267	13	Elimination of dead-time effects
G	267	267	13	Beam definition (anticoincidence with a hole)
S <sub>11</sub>	13	13	6.5	Beam scanning
S <sub>14</sub>	356	356	13	Testing
S <sub>15</sub>		o.d. 76	13	Testing
S <sub>13</sub> , A		711	25	Muon detection
S <sub>4</sub>		407	13	Transmission detection
S <sub>5</sub>		356	13	
S <sub>6</sub>		305	13	
S <sub>7</sub>		254	13	
S <sub>8</sub>		204	13	
S <sub>9</sub>		153	13	
S <sub>10</sub>		102	13	

<sup>6</sup> T. F. Kycia and E. W. Jenkins, *Nuclear Electronics* (International Atomic Energy Agency, Vienna, 1962), Vol. I, p. 63.

set was run with and the other without the anticoincidence signal from  $S_{13}$ . The results of this procedure will be discussed more fully later.

The electronics was kept at a temperature constant to  $\pm 1^\circ\text{C}$  and line regulated ac outlets were used where necessary. The high voltages on the photomultiplier tubes were maintained constant to  $\pm 2$  V. Checks of the efficiency of the transmission counters were carried out regularly throughout the data taking by switching the signal from the counter  $S_{15}$ , located behind the transmission counters, in coincidence with the input telescope signal. Other tests, such as scaler tests, tests of anticoincidence efficiency, etc., were done from time to time.

A possible source of electronic instability is the dependence on instantaneous counting rate. Such a dependence can have two main origins: accidental coincidences and dead time. These are discussed in the following sections.

3. *Accidental coincidences.* The effect due to accidentals comes about in the following way. A particle is absorbed in the target, but a second one arrives within the resolving time of the circuits and strikes a transmission counter. The absorption event is thus misinterpreted, and the measured cross section is decreased. In order to eliminate such events, two thick (13 mm) scintillation counters ( $D_1$  and  $D_2$  in Figs. 2 and 3) mounted on RCA 6810A photomultipliers giving slow linear-output pulses were inserted into the beam ahead of the hydrogen target. The signals were fed through discriminators with thresholds set for approximately 1.5 times the average pulse height for a single particle passing the counter. The signals from the two D counters were then put in coincidence and the resulting pulse was used to veto the input telescope coincidence. In this way, events involving two particles arriving within the unclipped pulse width of the RCA 6810A photomultipliers were eliminated. Two counters were used in coincidence in order to avoid elimination of single particles with an unusually large ionization (tail of the Landau distribution). It was possible by this means to reduce double-particle events by a factor of 100 (to a negligible level) while losing only 5% of the single-particle events.

4. *Circuit dead time.* One type of dead-time effect is manifested in the following way. A beam particle which does not trigger the  $\pi$  meson telescope strikes a transmission counter and will initiate a dead time in that transmission-counter channel. A second particle signalled by the input telescope then strikes the same detector and will fail to give a signal if it lags behind the first particle by more than the resolution time of the circuit but by less than the sum of the resolution and the dead time. This effect, if not taken into consideration, would introduce intensity-dependent fluctuations in the total cross section. To eliminate such an effect the T counter, which was large enough to intercept all beam particles expected to reach the detector, was included in the input telescope. It was mounted on an RCA 7746

photomultiplier tube. Its dead time was set at a value (34 nsec for Chronetic circuitry and 29 for BNL HEEP circuitry) which was larger than or equal to the dead time of all the transmission counters (33 nsec for Chronetic circuitry and 29 for HEEP circuitry). Its signal was added as a further coincidence requirement to the input telescope signal. When this counter was dead, no further events could be recorded. In this way transmission counter dead-time effects involving not more than two particles were eliminated.

The coincidence signal  $S_{1,2,3}$  in both HEEP and Chronetics were set to ignore a beam particle if it was preceded by another beam particle within 100 nsec in order to eliminate scaler dead-time effects.

5. *Beam-intensity variation.* In order to check the degree to which the equipment was still sensitive to rate-dependent effects, the positive pion-beam intensity was varied between 3000/burst and 80 000/burst by varying the vertical aperture of collimator 2. These rates were the counting rates of the pion telescope. The rates without the Čerenkov signal were twice as high, due to the protons in the beam. The counting rate of the telescope  $S_{1,2}$  was five times higher than the rate in  $S_{1,2,3}$ . The cross sections were measured for these different intensities. No significant systematic rate dependence was observed. However, with a positive beam at the highest intensities, somewhat increased fluctuations from point to point were observed which were attributed to variations in the duration of the accelerator beam spill on the target with consequent unusually high instantaneous rates. Some runs taken under these conditions of varying spill were repeated at reduced intensity.

### C. The Hydrogen Target

The liquid-hydrogen target was a modified version of that used by Galbraith *et al.*,<sup>7</sup> being a double-jacketed container composed of two concentric cylinders with the inner cylinder sealed off after filling. The modifications were designed to increase the density stability of the liquid hydrogen. A large reservoir (285 liters) for the outer jacket was added to extend the time between fillings to approximately four days. A pressure control was installed on the reservoir to keep the temperature of the hydrogen in the outer jacket sufficiently constant so that the density of the hydrogen in the inner container would change only by a negligible amount. This condition was achieved during most, but not all, of the data taking. However, the vapor pressure of the hydrogen in the inner container was monitored by a precision, temperature-compensated gauge which was read at least every hour. The absolute accuracy of this gauge was 0.025 psi, and it was sufficiently sensitive (0.01 psi), so that very accurate relative corrections could be

<sup>7</sup> W. Galbraith, E. W. Jenkins, T. F. Kycia, B. A. Leontic, R. H. Phillips, A. L. Read, and R. Rubinstein, *Phys. Rev.* **138**, B913 (1965).

made. A vapor pressure change of 0.1 psi is equivalent to a change in density of 0.033% ( $\sim 10 \mu\text{b}$  in the cross section). In addition, the pressure was continuously recorded on a strip chart which would have shown any short-term variation which occurred between the hourly readings. No such variations occurred which required correction of the data. After filling the reservoir, the system required about 6 h to reach usable stability as indicated by the pressure recording on the strip chart. In data analysis (Sec. V) all data were normalized to 18.00 psia (1.266 kg/cm<sup>2</sup>) and the largest adjustment for normalization of the total cross section amounted to 80  $\mu\text{b}$ . After filling, the pressure was always observed to decrease slowly, probably due to a minute leak in the pressure regulator. The maximum decrease during any given series of measurements was 63  $\mu\text{b}$ . A conservative estimate of the error in normalization is  $\pm 5 \mu\text{b}$ .

The length ( $\sim 3$  m) of the target was not ideal from the standpoint of multiple scattering but it was the only available one. However, since the main objective of the experiment was to search for structure as a function of momentum in the total cross section, it was decided at the outset to eliminate from the analysis data from any counters which showed effects of multiple scattering. On the other hand, the long target has the considerable advantage of providing more interaction path and thus, in a given time, leads to better statistical accuracy of the relative measurements.

The precise length of the target (305.6 cm) had previously<sup>7</sup> been determined to  $\pm 0.1\%$ . The only change made which might have affected the length was the replacement of the two 0.254-mm Mylar end windows with new ones, but previous measurements had shown that the difference in deflection between two different 0.254-mm Mylar windows was negligible. The target length filled with liquid hydrogen at 18.00 psia (1.266 kg/cm<sup>2</sup>) is equivalent to  $21.38 \pm 0.03 \text{ g cm}^{-2}$ , combining errors in the vapor pressure-density relationship,<sup>8</sup> vapor-pressure determination, normalization, effect of the shape of the deflected Mylar windows, and measurement of target length. Only variations in the vapor pressure affect relative-cross-section values and the error in observation of such variations is identical with that of normalization noted above, viz.,  $\pm 5 \mu\text{b}$ .

The beam size just before entry into the target was defined by counter S<sub>3</sub> (13.5 $\times$ 6.1 cm). Since the beam converged towards the transmission counters, the inner hydrogen container (14.6 cm diam) did not require very precise alignment. The target materials in the beam path, other than hydrogen, consisted of end windows and insulation and totaled 0.9 g cm<sup>-2</sup> of aluminum and 0.4 g cm<sup>-2</sup> of Mylar. Multiple scattering from this material was negligible compared to that from the hydrogen. The vacuum in the container surrounding the targets was maintained at  $\sim 10^{-5}$  mm Hg to eliminate possibility of condensation on the end windows.

<sup>8</sup> H. M. Roder, D. E. Diller, L. A. Weber, and R. D. Goodwin, *Cryogenics* 3, 16 (1963).

An identical dummy target was mounted beside the hydrogen target and differed only in that its inner container was under vacuum. Both targets were mounted on a frame which rolled on rails so that either target was easily positioned on the beam line. In order to ascertain that the two targets were really identical, a number of runs were taken with both inner containers empty but the outer containers filled with hydrogen as usual. The targets were interchanged regularly as in a normal run (see Sec. IV). In this way a difference of  $5 \pm 8 \mu\text{b}$  was found for the two targets, i.e., there is no measurable difference between them.

#### D. The Muon Veto

1. *Principles of the method.* The pion beam contains some muons and these will be transmitted through the target. If no precautions are taken, the measured total cross section will be lower than the true-pion cross section because of this contamination. The counter S<sub>13</sub> situated behind the iron absorber will, however, signal most of these events. Now some of the muons arise from pions which are transmitted through the target and which then decay between it and the transmission counters. Such a decay muon will either miss the detector at which the parent pion was aiming due to the muon-decay angle or, in the case where it reaches the detector, the transmission counter signal will be vetoed by the signal from counter S<sub>13</sub>. In both cases a genuine pion transmission event is counted as an interaction event. We can look upon this effect as an inefficiency in pion detection. As we have seen, such inefficiency does not affect the results, provided that it is the same for full and empty targets.

In fact, there is a small difference in decay probability between these two cases due to energy loss of the pion in the hydrogen. A correction can then be applied to the data, expressed by

$$\Delta\sigma = -Kd(l_D + \frac{1}{2}L)eL/p_0^2, \quad (8)$$

where

$$K = M/\rho LN, \quad (9)$$

and  $p_0$  is the incident momentum,  $d$  is the decay probability per unit length for particles of unit momentum,  $e$  is the momentum loss per unit length of target, and  $l_D$  is the decay path between the end of the hydrogen target to the beginning of the iron absorber.

The effect of this correction is to decrease the measured cross section by up to 100  $\mu\text{b}$ . Note that this correction does not require any knowledge of whether the decay muons miss or hit the detector. At first sight it seems perhaps more logical to apply the veto signal from S<sub>13</sub> to the input telescope rate so that muon events are ignored, rather than being counted as interaction events. In this case  $A$  would appear in both numerator and denominator of Eq. (1). The muons striking the target are indeed eliminated correctly in this way, but there are two disadvantages due to those muons

originating from decay behind the target. There would be a correction even in the absence of energy loss in the target because all incident pions which are transmitted and decay would be ignored, whereas some which interact (e.g., are scattered through a large angle) and decay would be counted. Thus a bias against transmission would be introduced. Moreover, one has to be sure in this case that even the muons missing the detectors are all intercepted by counter S<sub>13</sub> in spite of the multiple scattering in the iron, otherwise the correction which has to be applied becomes very complicated.

2. *Effect of iron thickness.* At a number of momenta, the iron thickness was varied from 15 to 153 cm. Figure 4 shows the measured cross section as a function of this thickness for 2.1-GeV/c positive pions. Similar curves were obtained at 3.0 and 4.0 GeV/c with the maximum shifted towards larger iron thickness. The shape of the curve is surprising at first sight. The fall off of the cross section towards large iron thickness is expected since muons are stopped, thereby preventing them from being vetoed. But the rise at small iron thickness cannot be understood in terms of muon absorption. It is assumed to be due to secondaries produced in the hydrogen at small angles which are of lower momentum than the beam pions and are more readily absorbed in the iron. Indeed, if the absorption of the beam pions in iron is described by an absorption coefficient  $\lambda$ , if the production rate of secondaries transmitted to detector  $i$  is  $a_i$ , and their absorption coefficient in iron  $\gamma > \lambda$ , then, excluding muon effects, we have

$$R_{ie} = R_{ie}^0(1 - e^{-\lambda t}), \quad (10)$$

$$R_{if} = R_{if}^0(1 - e^{-\lambda t}) + a_i(1 - e^{-\gamma t}), \quad (11)$$

where  $t$  is the iron thickness and the quantities with superscript 0 are the transmission rates for beam pions.

In this case the quantity  $\sigma_i = K \ln R_{ie}/R_{if}$  is a rising function of  $t$ . It is

$$K \ln \frac{R_{ie}^0}{R_{if}^0 + a_i \gamma / \lambda} \quad (12)$$

in the limit of small iron thickness, rising to

$$K \ln \frac{R_{ie}^0}{R_{if}^0 + a_i} \quad (13)$$

for large iron thickness, but never reaching the value  $K \ln(R_{ie}^0/R_{if}^0)$  corresponding to the behavior of beam particles only.

While these considerations permit a qualitative understanding of the dependence of measured cross section on iron thickness, it is not easy to find a satisfactory quantitative description and thereby to calculate for every momentum the correction leading from the measurements done at a given iron thickness to the absolute value of the cross section.

At low momenta the final data were taken near the optimum iron thickness and the correction is not ex-

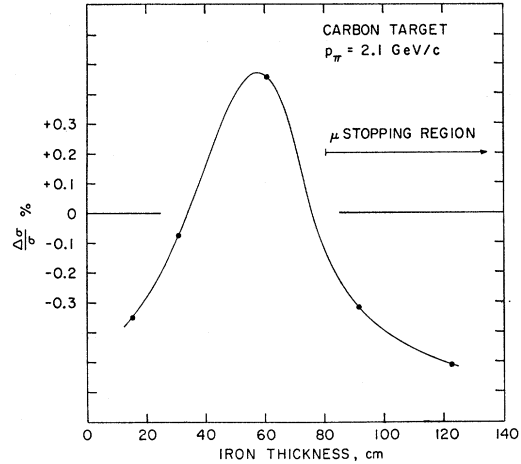


FIG. 4. The variation of the cross section with iron thickness; the line  $\Delta\sigma/\sigma=0$  is chosen arbitrarily.

pected to be too important. But it would have been necessary to keep adding iron when going to higher momenta in order to remain near to the optimum. Since we are searching for structure, we did not consider it advisable to change the iron thickness frequently. So we limited ourselves to one transition from 76 to 91 cm of iron at 3.0 GeV/c where this resulted in a step of less than 200  $\mu$ b.

These circumstances prove to be our most serious limitation in quoting an absolute cross section. We estimate this uncertainty to be  $\pm 0^{+400}$   $\mu$ b.

3. *An independent check.* Since the effects described in Sec. 2 above are momentum-dependent, it cannot be ruled out, *a priori*, that they may give rise to some structure in the measured cross section. In order to guard against such a possibility, most momentum intervals were covered also with runs when one set of electronics received no veto signal from counter S<sub>13</sub>. Such a measurement is obviously free from all the effects described but could be affected by a variation in muon contamination as a function of momentum. It was found that the curves obtained by the two methods

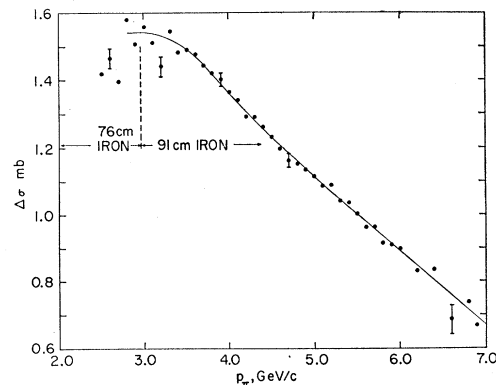


FIG. 5. The difference of  $\pi^-$  cross section with or without the muon veto.

were always similar in structure. Their separation is a measure of the muon contamination which is seen to decrease slowly as a function of momentum (see, e.g. Fig. 5).

#### IV. COLLECTION AND REDUCTION OF DATA

Whenever possible, a wide momentum region was covered by measuring the cross section, for particles of one sign, at points spaced by 100 MeV/c, increasing or decreasing the momentum monotonically. At the end of such a series, some points would be repeated as a check on reproducibility. Most regions were covered two or three times in this way.

As a further safeguard against instrumental effects, we measured the absorption cross sections of aluminum or of carbon at most momenta in addition to the hydrogen total cross section. Any instrumental effect giving rise to a structure would show up in these cross sections as well as in the hydrogen cross sections. Carbon was chosen because, from charge symmetry, the cross section for positive and negative pions is expected to be the same.

At a particular momentum a typical pattern of operations would be

*B T 4E 8F 8F 4E 8F 8F 4C 4C 4C 4E T*,

where *B* is the beam adjustment, *T* is an efficiency check of the transmission counters, *4E* is an empty target run with 4 million incident pions, *8F* is a full target run with 8 million incident pions, and *4C* is a carbon or aluminum target run with 4 million incident pions. Such a systematic pattern makes it possible to compare different runs taken at different times under identical conditions and to detect runs which deviate considerably from the others.

After each run the readings of all scalers and a code defining the momentum and the running conditions were printed out and also punched on paper tape. The data on the paper tape were subsequently converted to IBM cards.

The information was used to compute the transmission ratios and their normal statistical errors and to submit all ratios taken under identical conditions (including momentum repeats) to a consistency check. The  $\chi^2$  was worked out, which for good consistency should be of the order of the number of degrees of freedom, or the number of runs minus one. If the  $\chi^2$  turned out to be larger, the normal error was multiplied by a factor

$$[\chi^2/(\text{number of degrees of freedom})]^{1/2}$$

to give the "increased error." Finally the cross section was computed with errors based both on the normal and on the increased errors. When giving the results, the increased errors are always quoted.

A poor consistency can be caused either by random fluctuations that are nonstatistical (e.g., instrumental) with a period of the length of a run or shorter, or by a

trend or slow periodical variation. The uncertainty introduced by fast fluctuations is reduced, in the same way as the normal statistical error, by increasing the number of runs. Thus the increased error is a good measure of this uncertainty. For a *trend* the uncertainty is not reduced by increasing the number of runs so this uncertainty can, in principle, exceed that indicated by the increased error. But, in most cases, the average is over about four runs taken under identical conditions, so the uncertainty cannot be bigger than twice the increased error. This is still in line with the normal interpretation of an error so the increased error gives a good picture for the reliability of a measurement.

It should be noted that the cases in which the increased error was twice the statistical error or more were rare, and that in the majority of these cases some correlation with irregular operating conditions during a particular run (e.g., bad spill) could be made. Such runs (about two out of a thousand) were not included in the determination of the cross sections.

#### V. RESULTS

Three different sets of runs were carried out:

- (1) In a first set of runs the range 2.5–5.5 GeV/c was studied. The results of these runs have been published.<sup>9</sup>
- (2) In a second set of runs the range 2.1–6.9 GeV/c was studied. The preceding range was repeated and a higher momentum region was explored.
- (3) Some repeats were done in the 3.8–5.5-GeV/c range to improve the accuracy in regions where some small structure seemed to be detected.

In the present paper all the available data are combined. Before combining, corrections were made to allow for some systematic effects between two sets of

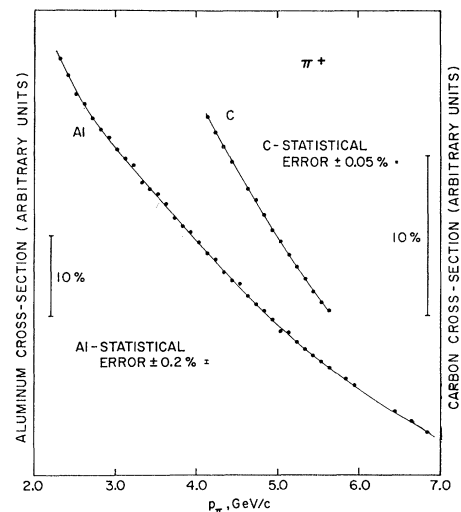


FIG. 6. Aluminum and carbon  $\pi^+$  total cross section.

<sup>9</sup> A. Citron, W. Galbraith, T. F. Kycia, B. A. Leontic, R. H. Phillips, and A. Rousset, Phys. Rev. Letters 13, 205 (1964).

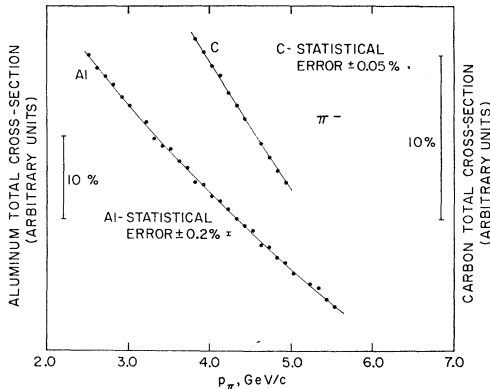


FIG. 7. Aluminum and carbon  $\pi^-$  total cross section.

data. The first correction is that due to a slow variation of the hydrogen density recorded by way of the equilibrium vapor pressure. After this correction a supplementary systematic correction was sometimes necessary to normalize two sets of data at the same average value. This correction (always smaller than  $100 \mu\text{b}$ ) was attributed to small alterations in the electronic equipment between two different measurements separated in time by several weeks. The variation of the electronics during one set of runs ( $\sim 3$  days) was checked with repeat points and found negligible. Corrections for Coulomb interference were applied from published data.<sup>10</sup>

For the combined runs, the statistical errors for individual points are about  $10 \mu\text{b}$  in the 3.8–5.5-GeV/c range and larger outside this range ( $\sim 25 \mu\text{b}$ ). These errors are a good estimate of the fluctuations from point to point. The dispersion of the points around the smooth curve is compatible with these errors.

The absence of instrumental fluctuation producing structure is demonstrated by the results on carbon and aluminum cross section (Figs. 6 and 7). They are smooth curves as expected from the smearing effects of the Fermi momentum and the  $T = \frac{1}{2}$  and  $T = \frac{3}{2}$  mixture.

The error for a measurement of the absolute values of total cross sections is much larger. This experiment was done essentially to detect structure in the cross sections and no particular care has been taken to get an absolute accuracy better than about 1%. The main contribution is given by the muon contamination (see Sec. III D2) and is estimated to about  $_{-0}^{+400} \mu\text{b}$ . Systematic effects influencing the extrapolation contribute also, and are estimated at  $\pm 200 \mu\text{b}$ .

An attempt has been made to derive precise values for the differences  $\sigma(\pi^- p) - \sigma(\pi^+ p)$  as a function of momentum because these quantities are used in dispersion relations to compute the real part of the forward charge-exchange amplitude. At a momentum of 3.3

GeV/c, two measurements were made consecutively, one of  $\sigma(\pi^+ p)$  and one of  $\sigma(\pi^- p)$ , with a minimum of change in conditions of the apparatus (only change in the sign of magnet currents) and in a minimum of time ( $\sim 4$  h). These measurements provide us the best estimate of the ratio  $\sigma(\pi^+ p)/\sigma(\pi^- p)$  eliminating the slow variations of the target and the electronics. After correcting the total set of data to obtain the same ratio  $\sigma(\pi^+ p)/\sigma(\pi^- p)$  at 3.3 GeV/c, the error in the difference between  $\pi^+ p$  and  $\pi^- p$  cross sections is then reduced to the statistical one. However, at least three uncertainties remain:

(a) The systematic effects introduced by the muon veto are assumed to be independent of the charge of the particle. This assumption has not been checked; the study of iron absorber effects was done only on positive pions. We estimate that the error is about a half that given for the absolute value, i.e.,  $_{-0}^{+200} \mu\text{b}$ .

(b) The residual proton contamination of the incident positive pions is assumed to be negligible. This has not been checked to an accuracy better than 1%. Such contamination, if present, could introduce an error of  $_{-100}^{+0} \mu\text{b}$ .

(c) Nuclear Coulomb interference effects<sup>10</sup> are different for  $\pi^+$  and  $\pi^-$ . A correction has been applied (see Appendix). The estimated uncertainty in this correction may be as great as  $\pm 150 \mu\text{b}$ .

It is estimated that the total systematic error in the difference  $\sigma(\pi^- p) - \sigma(\pi^+ p)$  is  $_{-200}^{+250} \mu\text{b}$ .

As a further check the carbon and aluminum data have been compared, taking into account in the case of

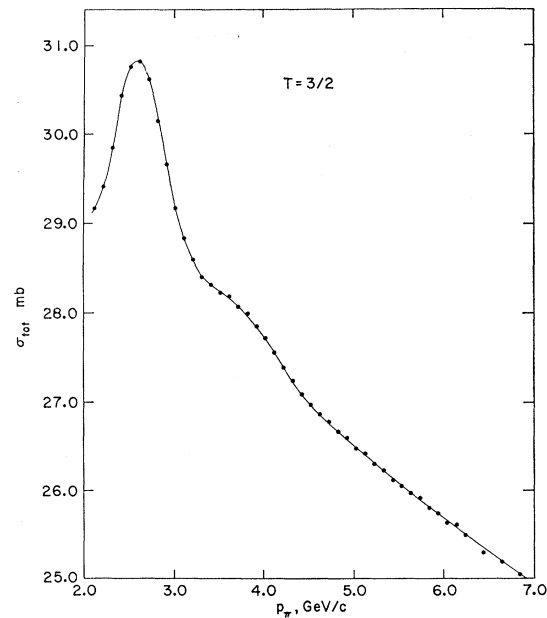
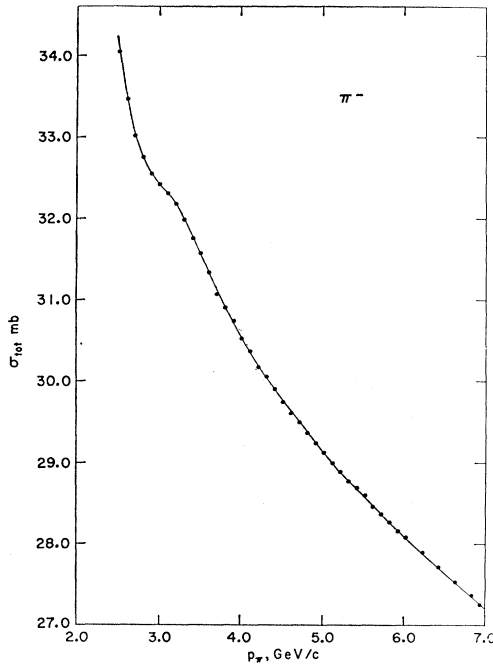


FIG. 8.  $T = \frac{3}{2}$ ,  $\pi^+$ , total cross section.

<sup>10</sup> K. J. Foley, R. S. Gilmore, R. S. Jones, S. J. Lindenbaum, W. A. Love, S. Ozaki, E. H. Willen, R. Yamada, and L. C. L. Yuan, in *Proceedings of the 12th International Conference on High-Energy Physics, Dubna, 1964* (Atomizdat, Moscow, 1965); Brookhaven National Laboratory Report No. BNL 8328 (unpublished).



$\pi^-$  TOTAL CROSS-SECTION  
FIG. 9.  $\pi^-$  total cross section.

aluminum the extra neutron. The results are

$$\begin{aligned} [\sigma(\pi^-Al) - \sigma(\pi^+Al)] / \sigma(\pi^+Al) &= (0.1 \pm 0.2)\% \\ [\sigma(\pi^-C) - \sigma(\pi^+C)] / \sigma(\pi^+C) &= (-0.6 \pm 0.1)\% \end{aligned}$$

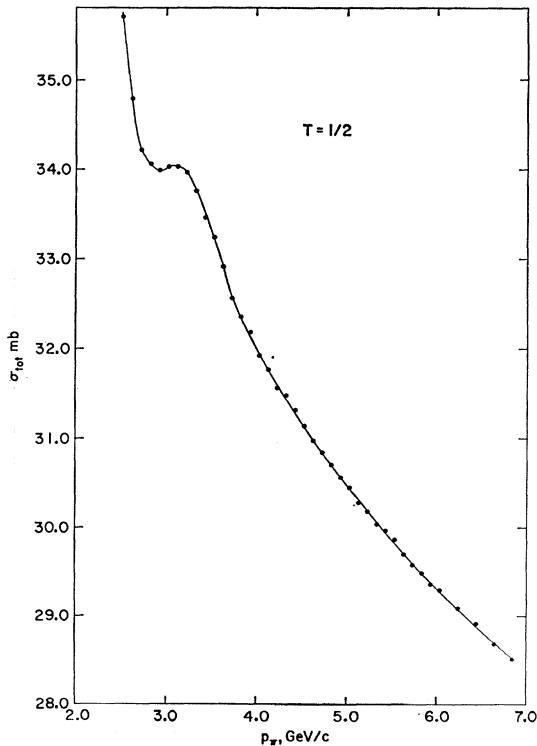


FIG. 10.  $T = \frac{1}{2}$  total cross section.

These results are in agreement with the possible systematic difference in the cross section for negative and positive pions.

The quantity  $\frac{1}{2}(k/4\pi)^2[\sigma(\pi^-p) - \sigma(\pi^+p)]^2$  has also been calculated (where  $k$  is the pion wave number in the c.m. system). This quantity is the contribution due to the imaginary part in the  $\pi^-p$  forward charge-exchange cross section.

The total cross section in the pure  $T = \frac{1}{2}$  has been calculated using the relation  $\sigma_{1/2} = \frac{1}{2}[3\sigma(\pi^-p) - \sigma(\pi^+p)]$ .

All the results have been tabulated in Table II and plotted in Figs. 8-12. The given errors are the statistical ones corresponding to fluctuation from point to point. As we have seen the absolute error in the  $\sigma(\pi^+p)$ ,  $\sigma(\pi^-p)$ , and  $\sigma(T = \frac{1}{2})$  is  $_{-200}^{+450} \mu\text{b}$  with a small additional error due to uncertainty in the electromagnetic corrections (see Appendix) and the systematic error in  $\sigma(\pi^-p) - \sigma(\pi^+p)$  is estimated to be  $_{-200}^{+250} \mu\text{b}$ .

The results have been compared with previous work<sup>1,2</sup> and found to be in reasonable agreement within the uncertainties.

## VI. DISCUSSION OF THE RESULTS

### A. The $N$ (2.65-GeV) and $\Delta$ (2.85-GeV) Bumps

Clearly the total-cross-section curves show bumps in the two isotopic spin states. The peaks are:

$$\begin{aligned} &\text{one in } T = \frac{1}{2} \text{ for } p_\pi \sim 3.3 \text{ GeV}/c \\ &\text{two in } T = \frac{3}{2} \text{ for } p_\pi \sim 2.6 \text{ GeV}/c \\ &\quad \text{and } p_\pi \sim 3.8 \text{ GeV}/c. \end{aligned}$$

The first  $T = \frac{3}{2}$  bump was observed two years ago by Diddens *et al.*<sup>1</sup> The two others are new.

The  $T = \frac{1}{2}$  bump is less apparent in the  $\sigma(\pi^-p)$  than in  $\sigma(T = \frac{1}{2})$ . This fact is essentially due to the regular recurrence of the  $T = \frac{1}{2}$  and  $T = \frac{3}{2}$  resonances. The admixture of  $T = \frac{3}{2}$  in  $\sigma(\pi^-p)$  and the presence of the two  $T = \frac{3}{2}$  resonances bounding the  $T = \frac{1}{2}$  one, smear it. The same effect produces enhancement of the valleys and bumps in the  $\sigma(\pi^-p) - \sigma(\pi^+p)$  curve.

### B. Determination of the Resonances Parameters

An attempt was made to determine, in a quantitative way, the position, the width, and the height of the bumps interpreted as resonances. The following Breit-Wigner formula was used to fit the bumps in the total-cross-section curves:

$$C(E^*) = 4\pi\lambda^2 \left( \frac{S}{4\pi\lambda_0^2} \right) \frac{\Gamma^2}{(E^* - E_0^*)^2 + \Gamma^2}, \quad (14)$$

where  $C(E^*)$  is the contribution of the resonances to the total cross section,  $\lambda$  is the wavelength of incident particles in the center-of-mass system,  $\lambda_0$  is the same quantity for resonance energy,  $E^*$  is the total energy of the  $\pi$ -nucleon system in the center-of-mass system,  $E_0^*$  is the mass  $M$  of the resonance,  $S$  is the height of the

TABLE II. Total cross sections.

$p_\pi$ (GeV/c)	$\sigma(\pi^+p)$ (mb)	$\sigma(\pi^-p)$ (mb)	$\sigma(T=\frac{1}{2})$ (mb)	$\sigma_{\pi^-}-\sigma_{\pi^+}$ (mb)	$\frac{1}{2}(k/4\pi)^2(\sigma_{\pi^-}-\sigma_{\pi^+})^2$ ( $\mu\text{b}/\text{sr}$ )
2.11	29.170±0.040	...	...	...	...
2.21	29.414±0.030	...	...	...	...
2.32	29.847±0.020	...	...	...	...
2.42	30.439±0.020	...	...	...	...
2.52	30.762±0.020	34.055±0.020	35.702±0.030	3.293±0.030	87.4±1.5
2.62	30.824±0.020	33.468±0.020	34.790±0.030	2.644±0.030	59.0±1.2
2.72	30.618±0.020	33.017±0.020	34.216±0.030	2.399±0.030	50.7±1.0
2.82	30.150±0.020	32.758±0.020	34.063±0.030	2.608±0.030	62.4±1.2
2.92	29.661±0.020	32.546±0.020	33.989±0.030	2.885±0.030	79.5±1.5
3.02	29.167±0.020	32.411±0.020	34.032±0.030	3.243±0.030	104.4±1.5
3.12	28.831±0.015	32.299±0.015	34.033±0.025	3.468±0.025	124.0±1.5
3.22	28.594±0.015	32.174±0.015	33.965±0.025	3.580±0.025	136.9±1.5
3.32	28.404±0.015	31.973±0.015	33.758±0.025	3.569±0.025	140.8±1.5
3.42	28.316±0.015	31.746±0.015	33.461±0.025	3.429±0.025	134.5±1.5
3.52	28.224±0.015	31.569±0.015	33.241±0.025	3.345±0.025	132.1±1.5
3.62	28.184±0.015	31.334±0.015	32.909±0.025	3.150±0.025	120.9±1.5
3.72	28.069±0.015	31.064±0.015	32.562±0.025	2.995±0.025	112.7±1.5
3.82	27.996±0.010	30.901±0.010	32.354±0.015	2.906±0.015	109.4±1.2
3.93	27.851±0.010	30.739±0.010	32.183±0.015	2.888±0.015	111.3±1.2
4.03	27.721±0.010	30.519±0.010	31.918±0.015	2.797±0.015	107.4±1.2
4.13	27.559±0.010	30.363±0.010	31.765±0.015	2.803±0.015	110.8±1.2
4.23	27.392±0.010	30.170±0.010	31.559±0.015	2.777±0.015	111.6±1.2
4.33	27.243±0.010	30.058±0.010	31.467±0.015	2.815±0.015	117.8±1.2
4.43	27.091±0.010	29.902±0.010	31.309±0.015	2.811±0.015	120.4±1.2
4.53	26.971±0.010	29.744±0.010	31.132±0.015	2.773±0.015	120.1±1.2
4.63	26.866±0.010	29.600±0.010	30.968±0.015	2.735±0.015	119.7±1.2
4.73	26.774±0.010	29.487±0.010	30.843±0.015	2.713±0.015	120.5±1.2
4.83	26.670±0.010	29.360±0.010	30.705±0.015	2.690±0.015	121.3±1.2
4.93	26.594±0.010	29.237±0.010	30.558±0.015	2.642±0.015	119.7±1.2
5.03	26.483±0.010	29.120±0.010	30.439±0.015	2.637±0.015	121.9±1.2
5.13	26.417±0.010	28.988±0.010	30.274±0.015	2.572±0.015	118.5±1.2
5.23	26.305±0.010	28.881±0.010	30.169±0.015	2.576±0.015	121.2±1.2
5.33	26.232±0.010	28.766±0.010	30.033±0.015	2.534±0.015	119.9±1.2
5.44	26.115±0.010	28.680±0.010	29.963±0.015	2.565±0.015	125.4±1.2
5.54	26.048±0.010	28.586±0.010	29.855±0.015	2.538±0.015	125.2±1.2
5.64	25.970±0.025	28.450±0.025	29.690±0.040	2.479±0.040	121.8±3.5
5.74	25.922±0.025	28.355±0.025	29.573±0.040	2.434±0.040	119.7±3.5
5.84	25.795±0.025	28.256±0.025	29.486±0.040	2.460±0.040	124.6±3.5
5.94	25.744±0.025	28.149±0.025	29.351±0.040	2.405±0.040	121.3±3.5
6.04	25.631±0.025	28.072±0.025	29.293±0.040	2.442±0.040	127.3±3.5
6.14	25.610±0.025	...	...	...	...
6.24	25.491±0.025	27.884±0.025	29.081±0.040	2.393±0.040	126.6±3.5
6.44	25.293±0.025	27.704±0.025	28.911±0.040	2.412±0.040	133.0±3.5
6.64	25.187±0.025	27.518±0.025	28.683±0.040	2.330±0.040	128.2±3.5
6.84	25.041±0.025	27.356±0.025	28.513±0.040	2.314±0.040	130.6±3.5
6.94	...	27.236±0.025	...	...	...

bump, and  $2\Gamma$  is the total width of the resonance. The justification for the use of this formula is not completely satisfactory. At least two assumptions are necessary:

- (1) The bumps in the total cross section are really due to resonances.
- (2) The nonresonant amplitude in the same orbital wave is assumed to have only slow variations near the resonance.

The fitting procedure consisted of variation of the three parameters  $S$ ,  $E_0^*$ , and  $\Gamma$  and a subtraction of the quantity  $C(E^*)$  from the experimental data to obtain a background as smooth as possible. This last requirement rests on an additional assumption that the background varies smoothly in the region of the resonance. The results are shown in Table III. The error on each parameter was estimated by looking for a significant

perturbation of the smooth background due to a variation of this parameter.

For the low-mass resonances, it has been the practice in the past to use a variable width  $\Gamma$  in relation (14) according to the formula

$$\Gamma = \gamma(p^*/p_0^*)^{2l+1}. \quad (15)$$

This formula is strictly applicable to purely elastic resonances and, for the present resonances which are probably inelastic, its validity is questionable.

TABLE III. Parameters of the resonances.

$T$	$p_\pi$ (GeV/c)	$E_0^*$ (mass) (GeV)	$2\Gamma$ (full width) (GeV)	$S$ (height) (mb)	$4\pi\lambda^2$ (mb)
$\frac{3}{2}$	2.65	2.423±0.010	0.310±0.020	3.150±0.10	4.495
$\frac{5}{2}$	3.84	2.850±0.012	0.400±0.040	0.77 ±0.06	2.944
$\frac{1}{2}$	3.256	2.649±0.010	0.360±0.020	1.55 ±0.10	3.554

Nevertheless, an attempt was made to fit the resonances in this way. The symmetrical shape of the bumps is incompatible with the shape given by Eq. (15) for large values of  $l$  ( $l \geq 2$ ). For small values of  $l$ , the asymmetry introduced by Eq. (15) can change the value of  $E_0^*$  by an amount of the order of  $\pm 0.03$  GeV. No account has been taken of this systematic effect in the errors given in Table II. The procedure adopted was to use a Breit-Wigner formula with a constant resonance width. Our data can be fitted adequately in this way.

The present results can be discussed in the light of other recent experimental work.

Evidence for structure in pion photoproduction<sup>11</sup> has been observed and interpreted as resulting from two pion-nucleon resonances, one with mass  $2.52 \pm 0.04$  GeV, probably in  $T = \frac{3}{2}$  state, and the other with mass 2.7 GeV in  $T = \frac{1}{2}$ . The observed structure may be due to the  $M = 2.423$  GeV and  $M = 2.65$  GeV with a shift introduced by an interference with the real part of amplitudes (as suggested by Höhler<sup>12</sup>).

$\pi^-p$  charge-exchange data observed in the forward direction also give an indication of structure.<sup>13</sup> There seems to be qualitative agreement between these data and the value of the expression  $\frac{1}{2}(k/4\pi)^2[\sigma(\pi^-p) - \sigma(\pi^+p)]^2$  as calculated from the data presented here (Fig. 12). There is, however, some quantitative disagreement on the momenta at which the resonances occur. The structure in the charge-exchange data has been interpreted by the authors as a  $T = \frac{1}{2}$  resonance at  $\sim 3.1$  GeV/ $c$  ( $E^* \sim 2.6$  GeV), or as two  $T = \frac{3}{2}$  resonances at  $\sim 2.6$  and  $3.5$  GeV/ $c$  ( $E^* \sim 2.4$  and  $2.7$  GeV) or as a combination of all three of these together. Our present data and previous results allow us to conclude that the structure observed in charge-exchange scattering can be explained as the combined effect of the three resonances at 2.423, 2.65, and 2.85 GeV. The discrepancy in energy, if real, could again be caused by a large momentum dependence in the difference of the real parts of the forward-scattering amplitudes  $\frac{1}{2}(D^- - D^+)^2$ .

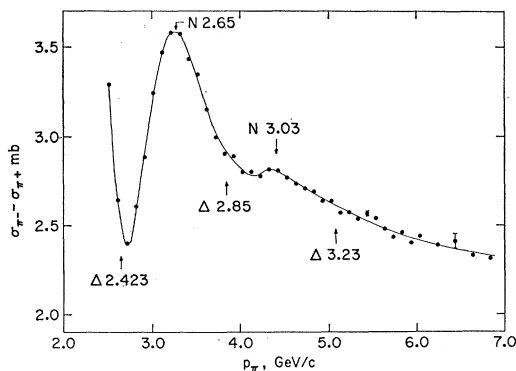


FIG. 11. The  $\pi^- - \pi^+$  cross-section difference.

<sup>11</sup> R. Alvarez, Z. Bar-Yam, W. Kern, D. Luckey, L. S. Osborne, S. Tazzari, and R. Fessel, Phys. Rev. Letters **12**, 710 (1964).

<sup>12</sup> G. Höhler and J. Giesecke, Phys. Letters **12**, 149 (1964).

<sup>13</sup> M. A. Wahlgig, I. Mannelli, L. Sodickson, O. Fackler, C. Ward, T. Kan, and E. Shibata, Phys. Rev. Letters **13**, 103 (1964).

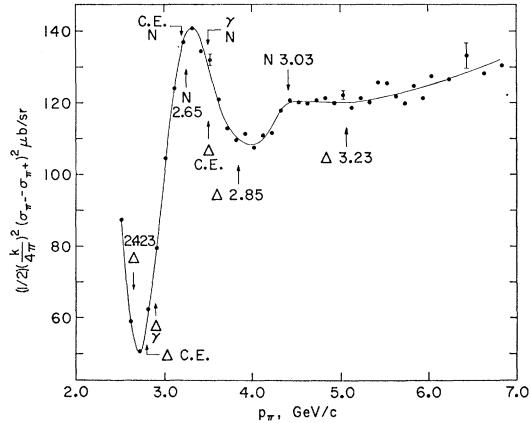


FIG. 12. The contribution of the imaginary amplitude in the forward charge-exchange (C.E.) cross section.

### C. Search for Other Resonances at Higher Momentum

Higher energy resonances are expected to be difficult to detect for at least three reasons:

- (1) The height of the bumps for  $p > 1.5$  GeV/ $c$  seems to be a monotonically decreasing function of the momentum.
- (2) The width in the center-of-mass system seems to be an increasing function of the momentum.
- (3) The width in the laboratory system is proportional to the mass of the resonances and therefore is increased even more.

These three independent phenomena contribute to the smearing of any possible bumps at higher momenta.

In the experimental total-cross-section curves there is no obvious bump within the range 4.0–7.0 GeV/ $c$ . Nevertheless, in this range, the curve has a curvature perhaps of the same order of magnitude as a possible bump (but with the inverse sign) and consequently makes the detection difficult. A part of this curvature is due to the tail of the preceding resonances. This part may be removed using the same technique as in the parameter determination. In doing so we must assume that the tail of a bump is described well by the tail of a Breit-Wigner formula. The experimental cross section curves (Figs. 13 and 14) after subtraction of the preceding resonances show another perturbation in the two isotopic spin states. The fitting of these two bumps with a Breit-Wigner formula yields the following parameters for these new resonances:

$$T = \frac{1}{2}, \quad M = 3.03 \text{ GeV}, \quad 2\Gamma = 0.400 \text{ GeV},$$

$$S = 0.150 \text{ mb},$$

$$T = \frac{3}{2}, \quad M = 3.23 \text{ GeV}, \quad 2\Gamma = 0.440 \text{ GeV},$$

$$S = 0.140 \text{ mb}.$$

The evidence for these two new bumps is strongly dependent on the two preceding ones because it appears

only after the subtraction. Many attempts were made to eliminate these new enhancements by changing the parameters of the subtracted preceding resonances but they always remained.

However, the observed bumps are very small and several assumptions about the applicability of the Breit-Wigner formula are necessary. In addition we cannot exclude with certainty a small undetected systematic effect responsible for such structure. Nevertheless our data can be interpreted as giving strong indications for two new resonances:

$$N (3.03 \text{ GeV}) \text{ and } \Delta (3.23 \text{ GeV}).$$

### VII. CONCLUSIONS

The experimental data on  $\pi^\pm$  total cross sections show two clear bumps in each of the two isotopic states. These two bumps cannot be due to systematic effects like muon contamination or intensity dependence and have been interpreted as pion-nucleon resonances. A fit with a Breit-Wigner formula has provided the parameters of these resonances: mass, width, and height. They explain in a qualitative way the results in photoproduction and  $\pi^-$  charge exchange.

After subtracting the Breit-Wigner fits to the two observed resonances, a clear indication of small structure, compatible with one resonance of higher mass in each of the isotopic states, is observed. We are unaware of any systematic effect that could cause such structure

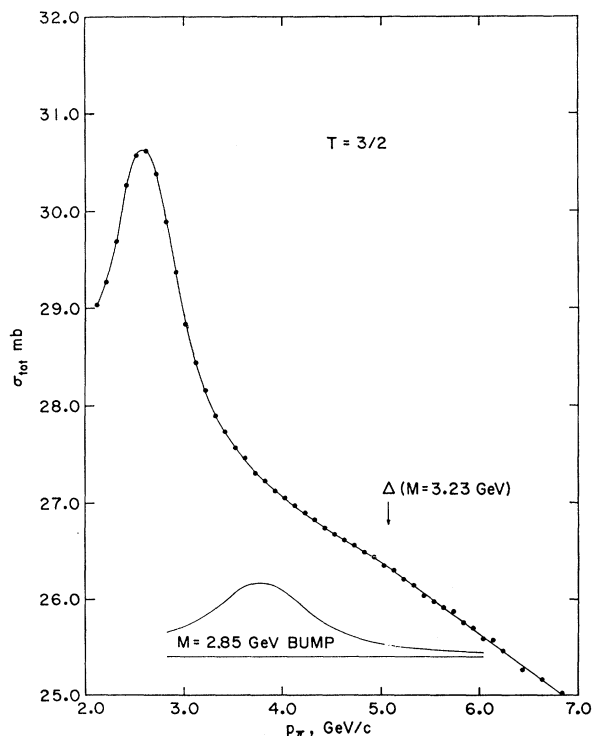


FIG. 13.  $T = \frac{3}{2}$  total cross section after subtraction of the  $M = 2.85$ -GeV bump.

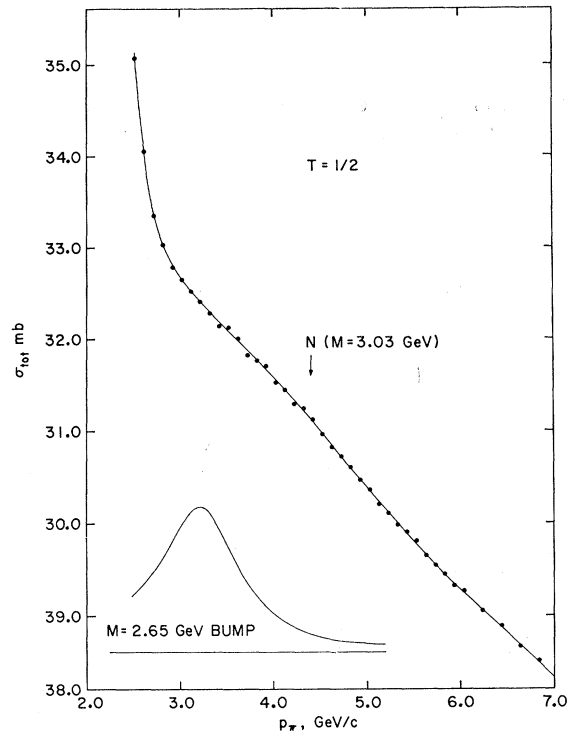


FIG. 14.  $T = \frac{1}{2}$  total cross section after subtraction of the  $M = 2.65$ -GeV bump.

but since the effect is so small, it would be desirable to see it confirmed by an independent experiment.

### ACKNOWLEDGMENTS

We wish to thank the following for their generous cooperation throughout the experiment: A. Schlafke, J. Gries, and members of the Cryogenic Group for the design, testing, and operation of the hydrogen targets throughout the run; G. Munoz, O. Thomas, H. Sauter, and F. Seier for technical assistance during the experiment; Dr. G. K. Green and the AGS staff, in particular Dr. T. F. Zipf, W. Walker, and T. Blair for their support and cooperation.

Finally we would like to thank Dr. R. L. Cool for the interest shown in this experiment and for helpful discussions.

### APPENDIX. ELECTROMAGNETIC CORRECTIONS TO THE TOTAL CROSS SECTION

The total cross section  $\sigma_i$  as observed with detector  $i$ , corresponds not only to nuclear processes, but also to single and multiple Coulomb scattering and to scattering due to interference between the real part of the elastic-scattering amplitude and the Coulomb-scattering amplitude. The detectors used for the extrapolation to zero solid angle are chosen in such a way that multiple scattering can be neglected. So we have only the tail of the single-scattering distribution and the interference

TABLE IV. Typical electromagnetic corrections.

Momentum (GeV/c)	Typical momentum transfer $t_i$ (GeV/c) <sup>2</sup>	Coulomb correction ( $\mu\text{b}$ )	Interference correc- tion $\pi^+$ ( $\mu\text{b}$ )	Total correc- tion $\pi^+$ ( $\mu\text{b}$ )	Total correc- tion $\pi^-$ ( $\mu\text{b}$ )	Total correction ( $\pi^-\pi^+$ ) ( $\mu\text{b}$ )
2.5	$6.24 \times 10^{-3}$	-40	-129	-169	102	271
4.5	$13.18 \times 10^{-3}$	-18	-84	-102	73	175
6.9	$31.0 \times 10^{-3}$	-6	-48	-55	44	98

scattering to take into account. In this way a correction arises:

$$\sigma - \sigma_i = - \int_{t_i}^{t_{\max}} \left( \frac{d\sigma}{dt} \right)_{\text{Coulomb}} dt - \int_{t_i}^{t_{\max}} \left( \frac{d\sigma}{dt} \right)_{\text{interference}} dt. \quad (\text{A1})$$

We now specify the differential cross sections used for  $\pi^\pm$  scattering:

$$\frac{d\sigma}{dt} = (1 + \xi^2) e^{\alpha + bt} + \left( \frac{d\sigma}{dt} \right)_{\text{inelastic}} + \frac{C^2}{t^2} \mp \frac{2C\xi}{t} e^{\alpha/2 + (b/2)t}, \quad (\text{A2})$$

where the terms on the right correspond to nuclear-elastic, nuclear-inelastic, Coulomb, and interference scattering, respectively; and where  $\xi$  is the (real part/imaginary part) of the forward-scattering amplitude (positive for an attractive potential),  $t$  is the four-momentum transfer (positive for physical scattering angles),  $e^\alpha$  is the contribution from the imaginary part to the forward elastic-scattering angles,  $b$  is a constant  $< 0$ , giving the fall off of the cross section, and  $C$  is  $2\pi^{1/2} r_0 m_e c = 5.12 \times 10^{-16}$  GeV/c cm, the constant for Rutherford scattering. With Eq. (A2), (A1) becomes

$$\sigma - \sigma_i = -C^2 \int_{t_i}^{t_{\max}} \frac{dt}{t^2} \pm 2C\xi e^{\alpha/2} \int_{t_i}^{t_{\max}} \frac{e^{(b/2)t}}{t} dt. \quad (\text{A3})$$

Here we have to make a restriction on  $t_{\max}$ . The formula (A2) is only valid for point charges. As soon as the proton form factor starts falling off appreciably, these terms decrease in importance. We express this by defining  $t_{\max}$  as the maximum transfer where the electromagnetic forces can be regarded as due to a point charge. In other words, we introduce a step-function form factor. For the Coulomb term we chose the momentum transfer where the square of the proton form factor falls to 0.5, namely  $t_{\max} = 0.12$  (GeV/c)<sup>2</sup>. For the interference term we have to take the point where the form factor itself falls to 0.5 and then find  $t_{\max}' = 0.24$  (GeV/c)<sup>2</sup>. It has been checked that this approximation of the form factor by a step function does not introduce an error larger than 10  $\mu\text{b}$  into the correction.

We now use the fact that for the published value<sup>8</sup>  $b \cong -9$  (GeV/c)<sup>-2</sup> and for the range of momentum transfers in question,  $|bt| \ll 1$ . Then we can develop and integrate

$$\sigma - \sigma_i = -C^2 \left( \frac{1}{t_i} - \frac{1}{t_{\max}} \right) \pm 2C\xi e^{\alpha/2} \times \left\{ \ln \frac{t_{\max}'}{t_i} + \frac{b}{2} (t_{\max}' - t_i) + \frac{b^2}{16} (t_{\max}'^2 - t_i^2) \right\}. \quad (\text{A4})$$

Our extrapolation procedure makes the term linear in  $t_i$  disappear and the quadratic term in  $t_i$  proves to be negligible, so there finally remains for  $\pi^\pm$

$$\sigma - \sigma_{\text{extrap}} = -C^2 \left( \frac{1}{t_i} - \frac{1}{t_{\max}} \right) \pm 2C\xi e^{\alpha/2} \times \left\{ \ln \frac{t_{\max}'}{t_i} + \frac{b}{2} t_{\max}' + \frac{b^2}{16} t_{\max}'^2 \right\}. \quad (\text{A5})$$

For  $\xi$  we use  $-0.2$  for all momenta, momentum transfers and signs in our range. This seems the best assumption for our present state of knowledge.<sup>9</sup> This is the largest source of uncertainty in the present estimate.  $e^{\alpha/2}$  follows from the optical theorem and the measured cross sections

$$e^{\alpha/2} = \sigma_\pm \frac{1}{4(\pi)^{1/2}} \frac{10^{13}}{0.197} = \frac{\sigma_\pm}{1.40} 10^{13} \text{ cm (GeV/c)}^{-1}.$$

So we obtain

$$\sigma - \sigma_{\text{extrap}} = - \frac{0.262}{t_i} + 2.2 \mp 1.45 \sigma_\pm \left\{ \ln \frac{0.24}{t_i} - 0.79 \right\} \mu\text{b}, \quad (\text{A6})$$

with  $t_i$  in (GeV/c)<sup>2</sup> and  $\sigma$  in millibarns. For  $t_i$  we use a momentum transfer typical for the counters actually used in the extrapolation.

Typical values for this correction are given in Table IV. The main uncertainty at this moment arises from the lack of precise information about the quantity  $\xi$ . We estimate this error to be  $\pm 50\%$ . Thus the corrections are uncertain by this amount.